J Fluoresc (2008) 18:1103–1114
DOI 10.1007/s10895-008-0360-z

ORIGINAL PAPER

Complexation of Dimethyl 2,3-Naphthalenedicarboxylate with 2-hydroxypropyl-α-, -β- and -γ-cyclodextrins in Aqueous Solution by Fluorescence, Circular Dichroism and Molecular Mechanics

Ruben Usero · Carolina Alvariza · María José González-Álvarez · Francisco Mendicuti

Received: 30 January 2008 / Accepted: 27 February 2008 / Published online: 4 June 2008

Abstract Fluorescence, circular dichroism and molecular mechanics have been used to study the complexation of 2,3-dimethyl naphthalenedicarboxylate with 2-hydroxypropyl-α-, -β and -γ-cyclodextrins (*HP*CDs) in aqueous solution. Emission spectra upon excitation of the naphthalenedicarboxylate group show two bands whose intensity ratio *R* is quite sensitive to polarity. From the change of *R* and lifetimes averages $<\tau>$ with *HP*CD concentration and temperature were obtained the stoichiometry, the association constants and the enthalpy and entropy changes during the complexation. *R*, $<\tau>$ and the fluorescence anisotropies (*r*) extrapolated at [*HP*CD]→∞ allows us to estimate the polarity and microviscosity of the media surrounding the guest when complexed. In addition, the analysis of quenching and induced circular dichroism experiments and molecular mechanics calculations in the presence of water, provide information about the forces responsible for the complexation and the geometry of the complexes.

Keywords Cyclodextrins · Inclusion complex · Fluorescence · Circular dichroism · 2,3-Napthalenedicarboxylate · 2,3-Dimethyl naphthoate · Molecular mechanics

R. Usero · C. Alvariza · M. J. González-Álvarez · F. Mendicuti (✉)
Departamento de Química Física, Universidad de Alcalá,
28871 Alcalá de Henares,
Madrid, Spain
e-mail: francisco.mendicuti@uah.es

Introduction

Cyclodextrins (CDs) are donut-shaped molecules capable of forming inclusion complexes with low molecular weight compounds and polymer guests [1–4]. CD cavities are relatively hydrophobic and the exterior surfaces are quite hydrophilic. Both microviscosity and polarity of the medium surrounding the guest molecule are substantially modified upon complexation. These changes frequently modify the spectroscopic characteristics of chromophore containing guests. Fluorescence emission intensity [5–13], excimer formation [14–18], fluorescence anisotropy [12, 19–22], the relative intensity of some bands of the emission spectra, [20–27] fluorescence decay [5, 8, 9, 12, 13, 21, 22, 27–29], energy transfer [30–32], fluorescence quenching [11–13, 20, 21, 30, 33], etc. may be affected upon inclusion. The analysis of the changes in these properties provides information about the structure of the complexes formed and allows us to determine quantitatively the stoichiometry, formation constants and thermodynamic parameters accompanying the association.

It is well-known that α-, β-, and γHPCD are chiral hosts that do not absorb in the UV–Vis region. However, an achiral chromophore guest may exhibit an induced circular dichroism (ICD) when forming a guest:CD complex [34]. In fact, ICD has also been used to determine the stability constants and stoichiometry for such complexes. In addition, ICD provides information about the geometry of the complex, as the sign and strength of the ICD signal are related to the distance and relative orientation of the guest with respect to the CD framework [35].

Molecular modeling [36], (molecular mechanics [10, 20, 27, 30, 37–42] and/or molecular dynamics [41–48]) has

also been extensively used as an additional tool for clarifying the inclusion mechanism as well as to extending the knowledge on the driving forces involved in such processes [1, 2].

Steady-state and time resolved fluorescence techniques combined with molecular mechanics calculations were used in a previous study on the complexation of 2,3-naphthalenedicarboxylate (*23*DMN) with natural α-, β- and γCDs [49]. Spectra for *23*DMN in the absence or in the presence of CDs exhibit two electronic bands whose ratio is very sensitive to the medium polarity. The association constants and the ΔH^0 and ΔS^0 were obtained from the change of this ratio with [CD] and temperature. All the complexes showed 1:1 stoichiometry. Binding constants at 25 °C for *23*DMN complexes with α-, β- and γCDs were 20±6, 1,060±25 and 40±10 M^{-1} respectively. Complexation with α- and βCDs exhibited $\Delta H^0<0$; the inclusion of *23*DMN into γCD showed $\Delta H^0>0$. Whereas the *23*DMN:αCD complex formation was accompanied by a $\Delta S^0<0$, the complexes with β- and γCD were achieved with a $\Delta S^0>0$. The $\Delta S^0<0$ was attributed to the partial *23*DMN penetration into the αCD; $\Delta S^0>0$ pointed towards a deep penetration of the guest into the β- and γCD cavities. Values of polarity surrounding *23*DMN in the complexes estimated from the values of *R* extrapolated at [CD]→∞, also agree with the latter statements. *23*DMN, in the complexes with α-, β- and γCDs, is surrounded by media with effective dielectric constants (ε) of 70, 49 and 58 respectively. ε for *23*DMN/βCD was similar to that expected for the inner βCD obtained previously with other similar probes; the one for *23*DMN/γCD implied that the γCD cavity is more polar [20–22, 25, 26]. However, the large value obtained for *23*DMN with αCD, whose cavity is well-known to be more hydrophobic, showed that a large portion of *23*DMN may be exposed to the water. These results may agree with the entropy changes, the extrapolated fluorescence anisotropy values and they might not disagree with the quenching experiments [49]. Molecular mechanics calculations also demonstrated that a strong repulsive energetic barrier impedes *23*DMN from entering inside the αCD cavity.

In a similar way the complexation of 2-methyl carboxylate (*2*MN) with 2-hydroxypropyl-α-, -β- and -γ-cyclodextrins was studied and compared with that of their natural counterparts α-, β- and γCDs [20, 21, 50]. Emission spectra of *2*MN also exhibited two typical bands. Results showed identical stoichiometry (1:1) for the three *2*MN complexes with α-, β- and γ*HP*CDs. Complexes with α- and β*HP*CDs resulted more stable than those formed with their counterparts α- and βCDs. Complexes with γ*HP*CD and γCD showed similar stability at 25 °C [20, 21]. Complexation of *2*MN with α*HP*CD is enthalpy driven, with β*HP*CD both the entropy and enthalpy terms favor the process, whereas the formation of the complex with γ*HP*CD is entropically governed. Complexation processes of *2*MN with natural CDs are accompanied by larger negative enthalpy changes than the ones obtained with their hydroxypropylated counterparts. The entropic terms accompanying the complexation, are more favorable (β- and γ*HP*CDs) or less unfavorable (α*HP*CDs) than with their natural counterparts. The differences in thermodynamics parameters upon complexation with respect to the natural CDs should mainly be caused by the differences in cavity sizes, which are apparently larger for the substituted CDs. Results revealed effective dielectric constants of the inner *HP*CD cavities of 51, 44 and 56 for α-, β- y γ*HP*CD respectively. These values differ from the α-, β-, and γCDs which behave more polar as the number of glucopyranose units increases [20]. Fluorescence anisotropy, quencher lifetimes, average lifetimes and molecular modeling also agreed with a total penetration of *2*MN inside the *HP*CD cavities.

In this work we investigate the complexation of *23*DMN with 2-hydroxypropyl-α-, -β and -γ-cyclodextrins (HPCDs) by using several steady-state and time-resolved fluorescence techniques, circular dichroism, as well as molecular mechanics calculations (MM). Stoichiometries, binding constants and ΔH^0 and ΔS^0, as well as information about the location of the guest in the complex, the polarity and microviscosity of the medium surrounding it, intermolecular interactions, etc. were obtained. Molecular mechanics methods were also used to support and strengthen most of the experimental evidence.

Materials and methods

Reagents and solutions

*23*DMN guest (Aldrich, 99%) and α-, β- and γHPCDs (Aldrich, 0.6 substitution degrees) were used as received. Karl–Fisher analysis for *HP*CDs revealed water contents by mass of approx. 7.0, 7.1 and 6.6% respectively. Deionized water (Milli-Q) and other solvents, *n*-alcohols $H(CH_2)_nOH$ with $n=1$–6 (Aldrich spectrophotometric grade or ≥98%) were checked for impurities by fluorescence before use. Water *23*DMN/*HP*CD solutions were prepared by weight from a doubly filtered (cellulose filters, Millipore, 1 μm ∅) guest saturated solution ([*23*DMN]=~10^{-7}M). [*HP*CD] ranged from 0 to 3.724×10^{-2}, 1.792×10^{-2} and 3.187×10^{-2} M for α-, β- and γ*HP*CD respectively. The contents of the cells were stirred for ~48 h prior measuring. For induced circular dichroism measurements, in order to avoid signal saturation at the wavelength of the maximum of the intense ^1B_b band (~245 nm), the stock *23*DMN guest solution was diluted approximately fifteen times.

Apparatus

Steady-state fluorescence measurements were recorded on an SLM 8100 Aminco Spectrofluorimeter equipped with a Xe lamp, a double (single) concave grating monochromator at the excitation (emission) path and Glan–Thompson prism polarizers in both paths. The photomultiplier was cooled by a Peltier system. The excitation and emission slit widths were 8 nm. The fluorescence decay measurements were achieved on a time correlated single photon counting (TCSPC) FL900 Edinburgh Instruments Spectrometer with a thyratron-gated lamp filled with H_2. Data acquisition was carried out by using a multichannel time detector and a time window width of 125 ns with a total of 10,000 counts at the intensity maximum. The instrumental response function was regularly obtained by measuring the scattering of a Ludox solution.

Induced circular dichroism (ICD) spectra were obtained by using a JASCO J-715 spectropolarimeter. Recorded spectra were the average of 2 scans taken at the speed of 5 nm/min with an 8 s time response. The bandwidth was set at 2 nm and the sensitivity and resolution were fixed at 20 mdeg and 0.2 nm respectively. All measurements were performed at 25 °C in 10 mm length cells.

Determination of association constants

Association constants for a 1:*n* guest:host complex (G: *HP*CD$_n$), whose global equilibrium can be written as

$$n\,HP\mathrm{CD} + 23\mathrm{DMN} \quad \rightleftarrows \quad 23\mathrm{DMN} : HP\mathrm{CD}_n \tag{1}$$

were determined by steady-state fluorescence measurements from the change of parameter R with [*HP*CD], by fitting the experimental data to the following equations [49]:

$$R = \frac{R_0 + R_\infty \Phi K [HP\mathrm{CD}]_0^n}{1 + \Phi K [HP\mathrm{CD}]_0^n} \tag{2}$$

and

$$\frac{1}{R - R_0} = \frac{1}{K\Phi(R_0 - R_\infty)} \frac{1}{[HP\mathrm{CD}]_0^n} + \frac{1}{R_0 - R_\infty} \tag{3}$$

where R_0 and R_∞ are the values of R for the free and complexed guest. R in both equations is defined as the $I(\lambda_2)/I(\lambda_1)$ ratio, by assuming that the emission spectra show bands whose intensity maxima are centered at λ_1 and λ_2. Thus $\Phi = I_\infty(\lambda_1)/I_0(\lambda_1)$, where $I_0(\lambda_1)$ and $I_\infty(\lambda_1)$ are the emission intensities (at λ_1) for the guest at [*HP*CD]=0 and extrapolated at [*HP*CD]→∞.

From the change with [*HP*CD] of the weighted average lifetime, defined as

$$\langle \tau \rangle = \frac{\sum_1^n A_i \tau_i^2}{\sum_1^n A_i \tau_i} \tag{4}$$

and obtained by the analysis of the multiple-exponential decay profiles of fluorescence intensity, the following equation is inferred

$$\langle \tau \rangle = \frac{\tau_0 + \tau_\infty K\Phi [HP\mathrm{CD}]_0^n}{1 + K\Phi [HP\mathrm{CD}]_0^n} \tag{5}$$

When lifetime measurements are collected at the emission wavelength λ_1, the parameter Φ from both Eqs. 2 and 5 has the same value.

From the steady-state fluorescence depolarization measurements (*L*-method) [51], the fluorescence anisotropy r can be quantified by

$$r = (I_{VV} - G I_{VH})/(I_{VV} + 2G I_{VH}) \tag{6}$$

I_{xy} is the intensity of the emission that is measured when the excitation polarizer is in position x (V for vertical, H for horizontal), the emission polarizer is in position y, and the G factor (= I_{HV}/I_{HH}) corrects for any depolarization produced by the optical system. Under the assumption that the total anisotropy is the sum of contributions due to uncomplexed and complexed guests, the following equation can be derived

$$r = \frac{r_0 + r_\infty K\Phi [HP\mathrm{CD}]}{1 + K\Phi [HP\mathrm{CD}]} \tag{7}$$

It contains the same Φ parameter as the previous equations when anisotropies are collected at λ_1 and at the same excitation wavelength.

The dynamic quenching of a single excited species by a quencher (Q) follows the known Stern–Volmer equation [52]. Even for simple systems, Stern–Volmer plots of steady-state measurements are usually non-linear, nevertheless they can give information about the quencher to chromophore accessibility.

Molecular mechanics (MM)

Calculations were performed with Sybyl 6.9 and the Tripos Force Field [53, 54]. A relative permittivity ε=1 was used in the vacuum and in the presence of water. Charges for *23*DMN were obtained by MOPAC [55]. Geometry and charges for water, *HP*CDs were identical to those previously used [50]. Initial *HP*CDs, fully substituted at C2 of the glucopyranose unit (molar substitution=1.0), and *23*DMN conformations were also taken from literature

[49, 50]. Non-bonded cut-off distances were set at 8 Å, the simplex algorithm and the conjugate gradient (0.2 and 1.0 kcal/mol Å in the vacuo and water respectively) were used as optimization and termination methods [56, 57]. The molecular silverware algorithm was employed for water solvation of the systems [58]. Periodic boundary conditions were also employed. Interaction energy was obtained as the difference between the potential energy of the whole system and the sum of the potential energies of the isolated components in the same structure.

Results and discussion

Fluorescence measurements

Excitation spectra (at 385 nm) for *23*DMN water solutions in the absence and in the presence of *HP*CDs showed bands at ~290 and ~335 nm. Emission spectra for *23*DMN and *23*DMN/HPCD water solutions recorded at λ_{ex}=282 nm, are depicted in Fig. 1. All spectra exhibit the two characteristic bands from naphthoate [20–22, 25–27, 39, 49] whose maxima slightly shifts to the blue upon increasing [*HP*CD]. Fluorescence intensity (area under emission spectrum) does not exhibit any special trend with [*HP*CD], as it increases or decreases depending on the host type. In addition, the spectra do not show any evidence of the inclusion of more than one *23*DMN inside *HP*CDs. Nevertheless, the main feature takes place in the ratio of intensities of both bands, which is strongly dependent on the medium polarity. Such bands are centered around 362± 2 nm (λ_1) and 383±2 nm (λ_2). The parameter R, measured as $I_{\sim 383\ nm}/I_{\sim 362\ nm}$, substantially varies with [*HP*CD] and temperature. The top of Fig. 2 depicts the decreasing in R with [*HP*CD] at different temperatures for the three systems. The shape of these curves suggests that complexes of *23*DMN with β*HP*CD are the most stable. Lines depicted in Fig. 2 come from the non-linear (top) and linear (bottom) adjustments of experimental data to Eqs. 2 and 3 respectively. The analysis agrees with a 1:1 stoichiometry and provides K, R_0 and R_∞ values by using $\Phi_{362\ nm}$ calculated at each temperature from the emission intensity at 362 nm in the absence of *HP*CD and at [*HP*CD]→∞. As Table 1 shows, $\Phi_{362}<1$ for *23*DMN/ αHPCD and *23*DMN/γHPCD systems whereas $\Phi_{362}>1$ for the *23*DMN/βHPCD one. In addition, Φ_{362} in the presence of β*HP*CD (γ*HP*CD) seems to decrease (increase) with temperature. The value for *23*DMN:αCD, however, is almost temperature independent. R_0 for *23*DMN at each temperature, as expected, are very similar for all systems. R_∞, however, depends on the *HP*CD type and temperature. At 25 °C R_0 is 0.99, whereas R_∞ are 0.79, 0.68 and 0.83 for α-, β- and γ*HP*CDs complexes. These values denote a decreasing in the medium polarity surrounding *23*DMN in the complex, which depends on the *HP*CD.

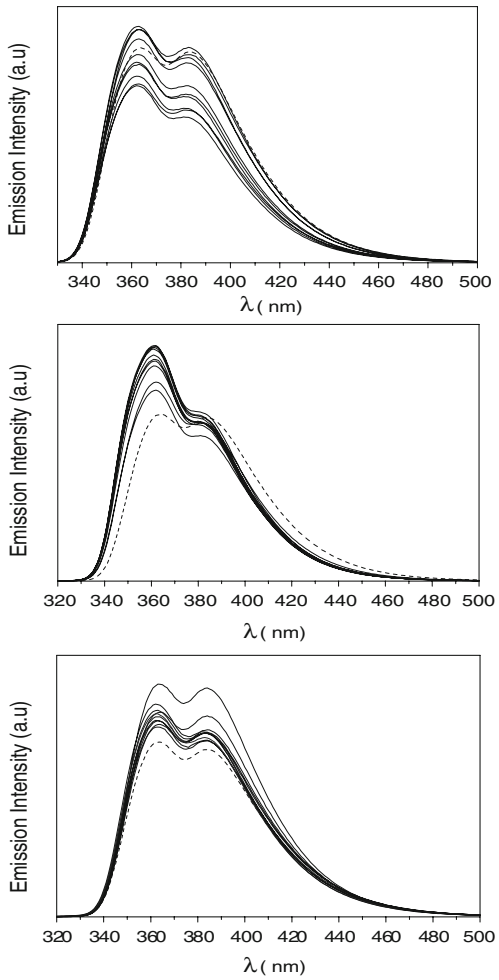

Fig. 1 Emission spectra for *23*DMN/α*HP*CD, 23DMN/β*HP*CD and 23DMN/γ*HP*CD systems at different [*HP*CD] concentrations at 25 °C. Concentrations range from 0 to 3.724×10^{-2}, 1.792×10^{-2} and 3.187×10^{-2} M for α-, β- and γ*HP*CD respectively. *Dashed curves* are for *23*DMN in the absence of *HP*CDs

The average of K are around 165, 1,080 and 80 M^{-1} for *23*DMN complexes with α-, β- and γ*HP*CDs at 25 °C. The value for *23*DMN:β*HP*CD at 25 °C is comparable to the one obtained for 23DMN:βCD (1,060 M^{-1}) [49]. The ones for *23*DMN:α*HP*CD and *23*DMN:γ*HP*CD are somewhat larger than the one observed for *23*DMN with the naturally occurring αCD (20 M^{-1}) and βCD (40 M^{-1}) [49].

Fluorescence intensity decay profiles (λ_{exc}=282 nm and λ_{em}=362 nm) for the *23*DMN water solutions were mono-exponentials, with a single fluorescence lifetime around 5 ns which hardly changes in the 5°–45 °C temperature range. Decays for *23*DMN/*HP*CD water solutions at any temperature and [*HP*CD] were fitted to the sum of two exponentials. As a result, two lifetime components, a short one close to the value for the free guest (5 ns) and a longer one attributed to the complexed form and whose value

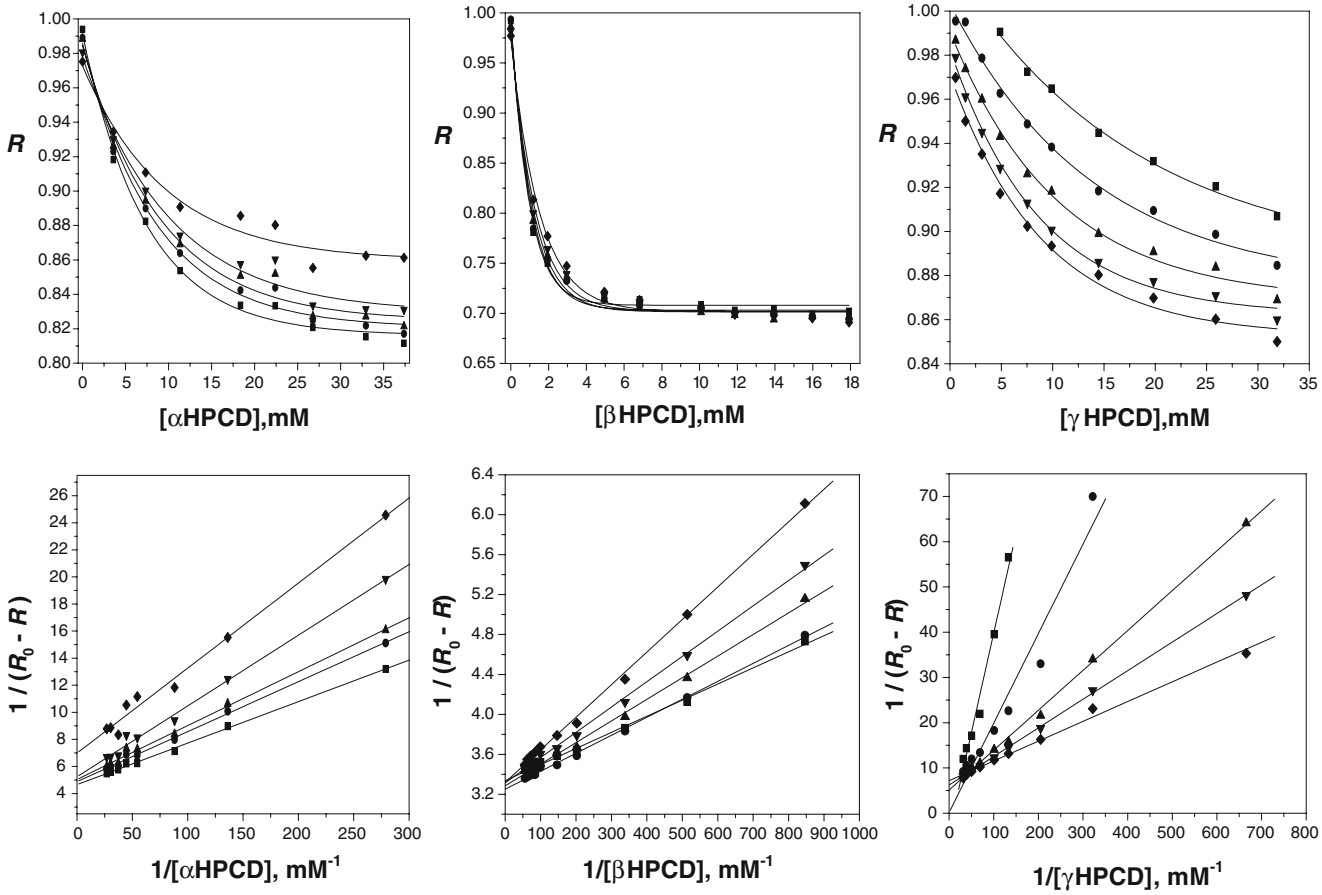

Fig. 2 (*Top*) Variation of *R* with [*HP*CD] and temperature. *Curves* are the result of the fitting by using Eq. 2; (*bottom*) double-reciprocal plots for *23*DMN guest complexes at different temperatures by fitting the data to Eq. 3. Symbols are a 5 °C (*filled square*), 15 °C (*filled circle*), 25 °C (*filled triangle*), 35 °C (*inverted filled triangle*) and 45 °C (*filled diamond*)

Table 1 Association constants *K*, obtained from the non-linear and linear adjustments (parentheses), R_0 and R_∞, as well as $\Phi_{362\ nm}$ for *23*DMN/α*HP*, *23*DMN/β*HP*CD and *23*DMN/γ*HP*CD systems at different temperatures

T (°C)	*K* (M^{-1})	$\Phi_{362\ nm}$	R_0	R_∞
*23*DMN/α*HP*CD				
5	213.1±15.3 (209.4±7.4)	0.73	0.994±0.003	0.780±0.004
15	163.3±16.9 (168.5±7.4)	0.78	0.989±0.004	0.782±0.006
25	158.8±23.8 (169.5±9.9)	0.75	0.988±0.005	0.786±0.008
35	149.7±28.6 (150.1±10.7)	0.67	0.980±0.006	0.789±0.011
45	150.7±40.4 (152.7±14.6)	0.73	0.975±0.007	0.831±0.011
*23*DMN/β*HP*CD				
5	1,676.6±51.9 (1,662.9±36.1)	1.45	0.992±0.002	0.693±0.001
15	1,292.5±35.1 (1,273.9±27.8)	1.42	0.993±0.002	0.686±0.001
25	1,100.7±38.5 (1,066.6±27.7)	1.42	0.986±0.002	0.683±0.001
35	1,035.8±29.7 (1,004.1±19.9)	1.30	0.982±0.002	0.681±0.001
45	841.1±26.9 (817.4±20.4)	1.25	0.977±0.001	0.677±0.001
*23*DMN/γ*HP*CD				
5	60.7 ±15.2 (–±–)	0.83	1.028±0.008	0.834±0.016
15	66.1±10.7 (44.8±4.9)	0.90	1.005±0.003	0.825±0.012
25	95.8±11.2 (76.3±6.5)	0.95	0.994±0.003	0.831±0.006
35	112.3±8.7 (103.3±5.1)	0.99	0.985±0.002	0.828±0.004
45	115.4 ±9.3 (112.5±8.7)	1.07	0.977±0.002	0.822±0.004

depends on the CD type, were obtained. Figure 3 depicts the variation of the lifetime averages, as $\langle\tau\rangle/\tau_0$, with [*HP*CD] for one of the systems at several temperatures (top) and for the three systems at 25 °C (bottom). Curves show the result of the adjustments to a rearranged Eq. 5, by using Φ_{362} values obtained from steady-state measurements. *K*'s obtained from this analysis are reasonably similar to the ones from steady state, *i.e.*, 180±17, 930±35 and 115±24 M^{-1} for complexation with α-, β- and γ*HP*CD respectively at 25 °C. Values of τ_∞, at the same temperature, are 6.7, 7.4 and 6.5 ns respectively. These values together with R_∞ (0.79, 0.68, 0.83) for α-, β- and γ*HP*CDs respectively at 25 °C can provide information about the microviscosity and polarity of the medium surrounding *23*DMN when complexed. For this purpose the dependence of R and τ on the polarity (ε) and microviscosity (η) was obtained by performing emission spectra and time-resolved measurements for *23*DMN dilute solutions of different hydroxypropylated solvents covering a wide range of ε and η at 25 °C [49]. Emission spectra showed the two typical bands and intensity decays are mono-exponential for any of the solvents used. R increases monotonically with ε according the following quadratic equation $R = 0.55 + 5.32 \times 10^{-4}\varepsilon + 6.14 \times 10^{-5}\varepsilon^2$, where-

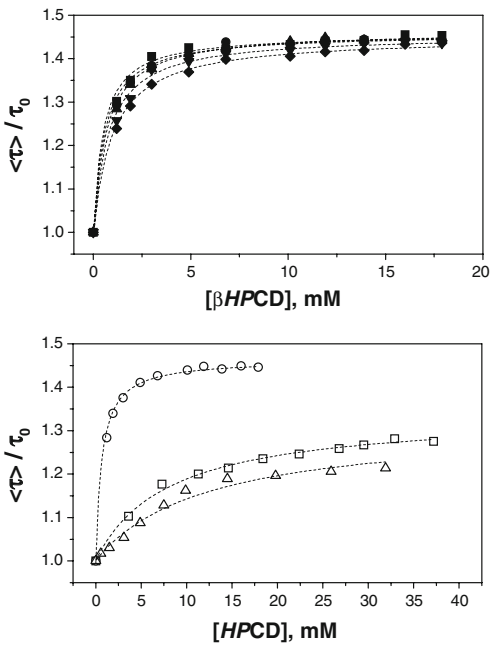

Fig. 3 (*Top*) Changes in the average lifetime, $\langle\tau\rangle$ with [β*HP*CD] and temperature: Symbols are a 5 °C (*filled square*), 15 °C (*filled circle*), 25 °C (*filled triangle*), 35 °C (*inverted filled triangle*) and 45 °C (*filled diamond*); (*Bottom*) variation in $\langle\tau\rangle$ with [α*HP*CD] (*empty square*), [β*HP*CD] (*empty circle*) and [γ*HP*CD] (*empty triangle*) at 25 °C. *Curves* fit the experimental data to the Eq. 5 by assuming $\Phi_{362\ nm}$ values obtained from the emission spectra; (λ_{em}=362 nm, λ_{ex}= 282 nm). These fits provide values for *K* at 25 °C of 178.0±17.4; 929.8±34.5 and 115.1±24.0 M^{-1} for *23*DMN complexes with α-, β- and γ*HP*CDs respectively

as it hardly changes with η at the same temperature. τ, however, decreases with ε and it increases almost linearly with η.

Effective dielectric constants (ε) for the media surrounding *23*DMN in the complexes with α-, β- and γ*HP*CDs of 58, 41 and 63 were estimated from R_∞ and the above equation. These values are quite similar to those obtained when *2*MN complexes with α-, β- and γ*HP*CDs (51, 44 and 56 respectively) [21]. Something different occurs when *23*DMN complexes with their counterparts α-, β- and γCD [49]. The value for *23*DMN/αCD ($\varepsilon\approx70$) substantially differs from that for *23*DMN/α*HP*CD. *23*DMN partially penetrates in the most hydrophobic αCD cavity and totally in the β- and γCD ones [49]. However, *2*MN, which is less bulky than *23*DMN, seems to deeply penetrate inside the three α-, β- and γ*HP*CDs. Thus ε values, that which are very similar ($\varepsilon\approx50$), correspond to the ones for the inner α-, β- and γ*HP*CD cavities. This contrasts with the natural CDs whose polarities are rather different (around 6, 50 and 70) [20, 21, 50]. As $\langle\tau\rangle/\tau_0$ increases with [*HP*CD] (and $\tau_\infty > \tau_0$), this increase may be attributed to the η increases and the ε decreases around the guest upon complexation. The largest τ_∞ obtained for *23*DMN/β*HP*CD as compared to the other two complexes, may be a consequence of the highest microviscosity surrounding a guest that is deeply trapped inside a cavity with a relatively low ε (= 44).

ΔH^0 and ΔS^0 were obtained from the average of *K* constants from steady-state measurements by using the linear van't Hoff representations depicted in Fig. 4. The results of the analysis were collected in Table 2 and compared with the thermodynamic parameters for *23*DMN complexation with the unsubstituted CDs [49]. Inclusion processes for *23*DMN with α- and β*HP*CDs have $\Delta H^0<0$, but are slightly more favorable for the *23*DMN/β*HP*CD complex. The *23*DMN:γCD is accompanied by an unfavorable positive enthalpy change. The signs of ΔH^0 match those obtained for complexation with their natural CDs, however absolute values are smaller as a consequence

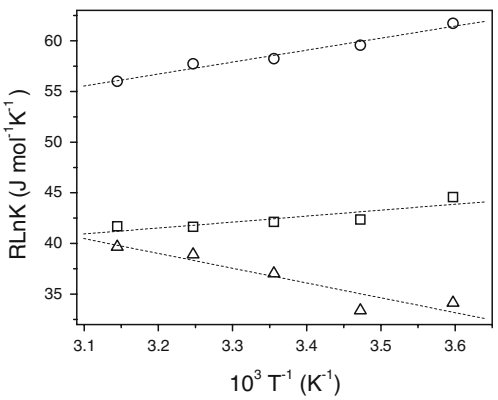

Fig. 4 Van't Hoff representations for the formation of the 1:1 stoichiometry 23DMN:α*HP*CD (*empty square*), 23DMN:β*HP*CD (*empty circle*) and 23DMN:γ*HP*CD (*empty triangle*) complexes

Table 2 Thermodynamics parameters obtained from the average of the constants collected in Table 1 from non-linear and linear fits at different temperatures

Complex	ΔH^0 (kJ mol^{-1})	ΔS^0 (JK^{-1} mol^{-1})
α*HP*CD	−7.8±2.5	+15.9±8.7
(αCD)	(−9.1±5.2)	(−4.8±15.0)
β*HP*CD	−12.0±1.2	+18.1±4.1
(βCD)	(−15.7±1.6)	(+6.0±5.6)
γ*HP*CD	+14.1±3.3	+83.9±11.1
(γCD)	(+35.2±7.5)	(+145.9±25.2)

In parentheses are the values obtained for the complexes of *23*DMN with α-, β- and γCDs from Ref. [49]

of the probably weaker guest/host interactions due to their larger cavity sizes.

The entropic terms accompanying the complexation are favourable for any of the *23*DMN/*HP*CD complexes. Something similar occurred when *23*DMN complexes with β- and γCDs, but it contrasts with the result obtained when it complexes with αCD. This complexation was accompanied by a small negative entropy change [39, 49]. $\Delta S^0<0$ values are typically obtained for guests that partially penetrate inside the CD cavity and/or whose movement is hindered by strong intermolecular guest-CD interactions. A guest that penetrates into the cavity exhibits $\Delta S^0>0$. The entropy sign is normally the result of two opposite effects, the loss of the solvent order surrounding the guest or included inside the CD host, and the decrease in the degrees of freedom of the guest due to its association with the host upon complexation. Thermodynamic parameters together with the values of R_∞ may agree with a good penetration of *23*DMN inside any of the three hydroxypropylated hosts. The placement of the guest would depend on the *HP*CD size.

Figure 5 depicts changes in *r* with [*HP*CD] for *23*DMN/β*HP*CD at different temperatures and for the three systems at 25 °C. Curves are the results of the adjustments, which seem to fit reasonably, of experimental anisotropy data to Eq. 7 by using *K* and *Φ* values from steady-state. *r* increases as [β*HP*CD] increases because of the larger fraction of the complexed form which has a smaller rotational diffusion rate than free *23*DMN and it decreases with temperature. This is probably due to a decrease in the solvent viscosity with temperature instead of the decrease in the fraction of the complex, as this trend is also observed for 23DMN/γ*HP*CD, whose complexation is accompanied by $\Delta H^0>0$. Values at [*HP*CD]→∞ (R_∞) at 25 °C obtained from the adjustments to Eq. 7, are 0.0062±0.0002, 0.0034±0.0002 and 0.0097±0.0004 for complexes with α-, β- and γ*HP*CDs respectively. These values, which follow the same trend as when *23*DMN complexes with unsubstituted CDs [49], are obviously larger than those obtained for the free *23*DMN guest ($r_0\approx7\times10^{-4}$). By assuming that the whole complex, where *23*DMN is located inside the cavity, moves as a whole, the larger value for R_∞ (γ*HP*CD)>R_∞ (β*HP*CD) may be related to the size of the complex. However, the relatively large R_∞ (α*HP*CD) value may agree with the fact that *23*DMN would not totally be include inside α*HP*CD but tightly bonded to it, making the size of the complex relatively large.

Quencher measurements at 25 °C were performed on *23*DMN and *23*DMN/HPCD water solutions for a 0.75 fraction of the guest complexed by using a solution of diacetyl, $(CH_3CO)_2$ (1 M), as quencher. Emission intensity obviously decreases upon quencher addition, but *R* remains almost constant (the presence of the quencher does not substantially modify the structure of the complexes). Figure 6 shows Stern–Volmer representations for the *23*DMN and *23*DMN/*HP*CDs, which in the range of quencher concentration are non-linear. The results agree with the fact that the free *23*DMN is much more accessible to the quencher than the complexed one. But they also reveal, in agreement with a not total penetration of *23*DMN into the α*HP*CD cavity, that the accessibility of *23*DMN in the complex with α*HP*CD is larger than with β*HP*CD, and this in turn is larger than when it complexes with γ*HP*CD.

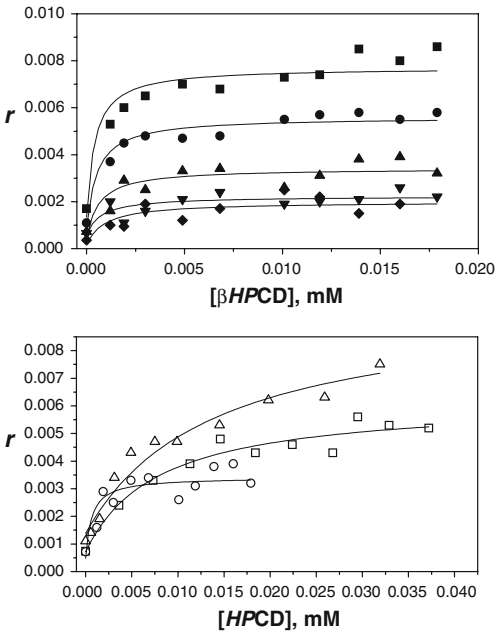

Fig. 5 (*Top*) Variation of the fluorescence anisotropy, *r* with [β*HP*CD] at different temperatures: 5 °C (*filled square*), 15 °C (*filled circle*), 25 °C (*filled triangle*), 35 °C (*inverted filled triangle*) and 45 °C (*filled diamond*), measured at the maximum of the low energy band (λ_{em}= 362 nm, λ_{ex}=282 nm); (*bottom*) variation of *r* with [α*HP*CD] (*empty square*), [β*HP*CD] (*empty circle*) and [γ*HP*CD] (*empty triangle*) at 25 °C

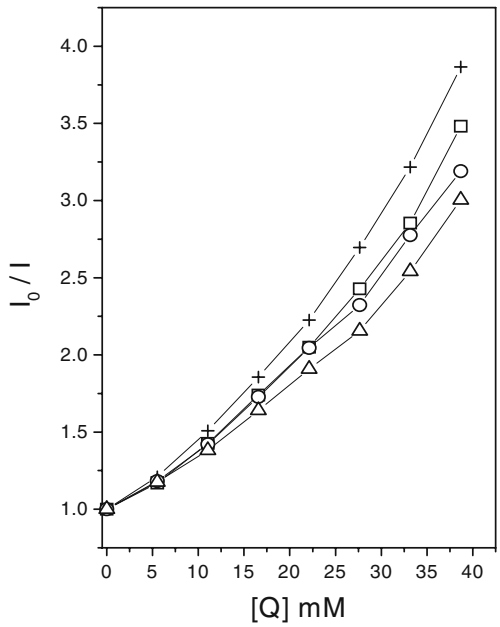

Fig. 6 Stern–Volmer plots from steady-state (fluorescence intensity) at 25 °C by using diacetyl as quencher of *23*DMN (*plus sign*) and *23*DMN:α*HP*CD (*empty square*), 23DMN:β*HP*CD (*empty circle*) and 23DMN:γ*HP*CD (*empty triangle*) water solutions. Solutions were for a [*HP*CD] which provides a 0.75 fraction of the complexed guest

Circular dichroism measurements

Absorption spectrum for free *23*DMN or in the presence of HPCDs exhibits three main bands placed at approximately 245, 282 and 320 nm which, according to the Platt's notation, were ascribed to the ^1B_b, ^1L_a and ^1L_b bands respectively [59]. Transition moments are nearly parallel to the long naphthalene axis for ^1B_b and to the short one for ^1L_a and ^1L_b bands [60, 61]. Figure 7 depicts ICD spectra at 25 °C for isolated *23*DMN and *23*DMN/*HP*CD water solutions, upon selecting the intense ^1B_b naphthalene absorption band. All *23*DMN/*HP*CD solutions were prepared for a 0.7 fraction of the complexed guest. Figure 7 also shows the absorption spectrum for *23*DMN. The ICD spectrum for both *23*DMN/βHPCD and *23*DMN/γHPCD exhibits a positive band. This band is substantially more intense for the former one. A weak negative one is obtained for the *23*DMN/αHPCD solution and the ICD spectrum for the isolated *23*DMN guest is obviously not observed. When focussing on the ^1L_a band (~275 nm) for *23*DMN/βHPCD at a higher *23*DMN concentration, a faint negative band is obtained.

The ICD spectrum sign varies depending on the inclusion of the chromophore in the CD cavity and the orientation of its electronic transition moment relative to the CD *n*-fold rotational axis. Parallel (perpendicular) orientation gives a positive (negative) ICD band [34, 35, 62–65]. A large intensity is usually related to a better fit of the chromophore into de CD cavity. In addition, the sign of the ICD when the chromophore is located partially outside the cavity becomes opposite to the inside one [66–68]. The positive ICD spectra for β- and γHPCDs suggest that *23*DMN guests are axially oriented, *i.e*, long naphthalene axis nearly parallel to the *n*-fold rotation CD axis. This is corroborated by the change of ICD sign for the ^1L_a band. In addition, the high intensity of the *23*DMN/β*HP*CD ^1B_b band suggests a better fit and deep penetration of *23*DMN inside β*HP*CD, whose movement is probably quite hindered. The decreasing in intensity for the complex with γ*HP*CD probably comes from the increase in the cavity size resulting in a fit that is slightly worse [67, 69]. In contrast, the weak negative ICD band for the *23*DMN/αHPCD solution agrees, either with the fact that *23*DMN do not penetrate totally inside the cavity, or that the 23DMN is equatorially oriented in the inner *HP*CD cavity, which is rather improbable [60].

A non-linear equation similar to Eqs. 2, 5 and 7, derived by assuming an ellipticity zero for free *23*DMN and $\Phi=1$, can also provide association constants. Experimental data adjust nicely to the non-linear equation showing $K = 910 \pm 50\ M^{-1}$ for *23*DMN/β*HP*CD at 25 °C, which reasonably agrees with those obtained from different fluorescence techniques.

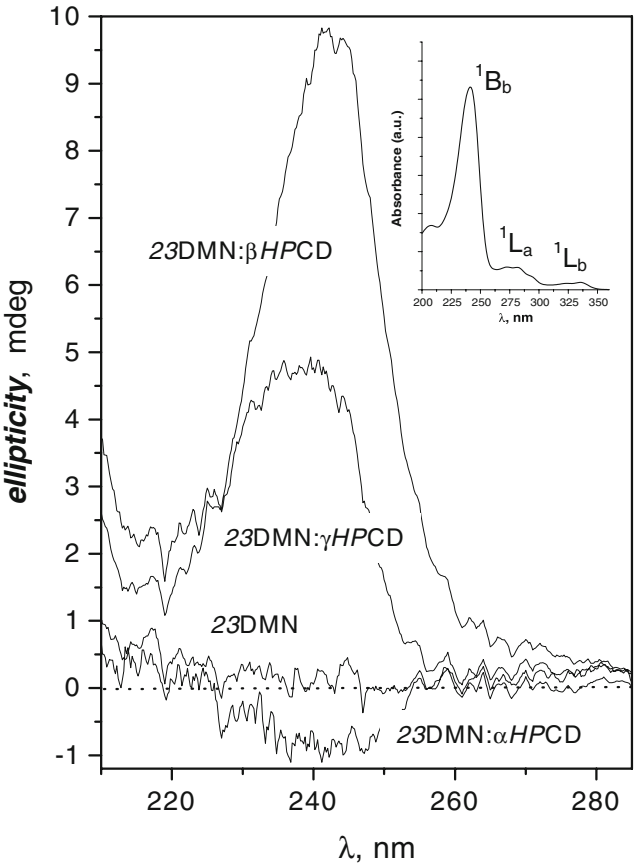

Fig. 7 Circular dichroism spectra of *23*DMN and *23*DMN in the presence of α-, β- and γ*HP*CD water solutions (prepared for a [*HP*CD] which provides a 0.7 fraction of complexed guest)

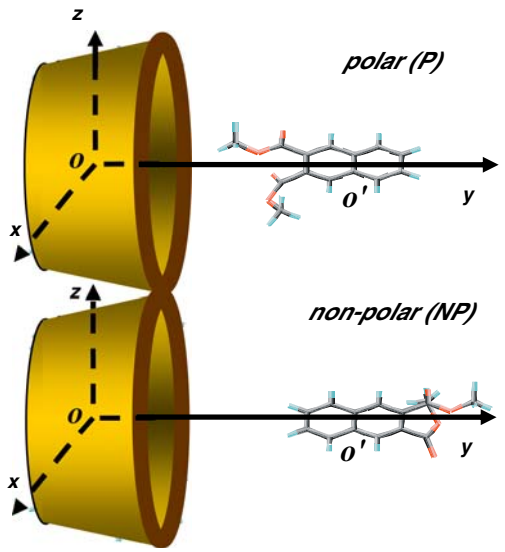

Fig. 8 Coordinate systems used to follow the (1:1) *23*DMN complexation process with *HP*CDs by polar and non-polar guest-to-host approaching

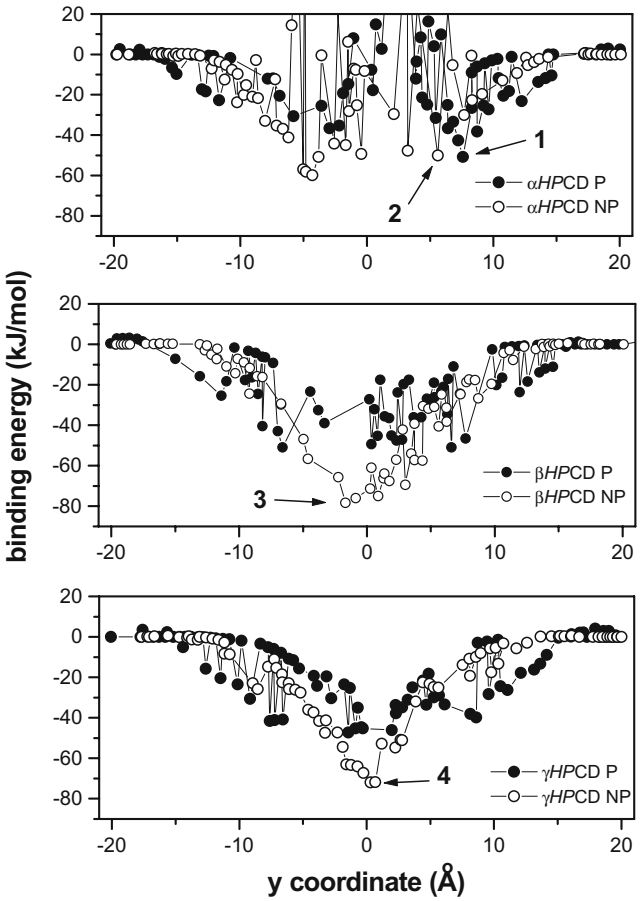

Fig. 9 Binding energies as a function of guest-host distance *d* (in Å) for *23*DMN complexation processes with α- (*top*), β- (*middle*) and γCDs (*bottom* panel) by polar (*P*; *filled circle*) and non-polar (*NP*; *empty circle*) guest-to-host approaching

Molecular mechanics calculations

Each *HP*CD was initially placed so that the center of mass of the glycosidic oxygen atoms (denoted by o in Fig. 8) was located at the origin of a coordinate system with its axis oriented as depicted [49, 50]. The *23*DMN guest was then approached to the *HP*CD by the polar (*P*) and non-polar (*NP*) sides as shown in Fig. 8. The host-guest distance was measured as the *oo'* projection (*d*) on the y axis. The inclusion torsional angle (θ) was measured between the *yz* and *oo'*C9 (C9 from naphthalene group) planes. The *oo'*C9 angle (δ) also contributes to defining the orientation of *23*DMN relative to the *y* axis. To obtain the most favorable approach of the guest, binding energies of all the optimized structures in the vacuum obtained by scanning δ and θ angles, in the 10–100° and 0–55° ranges respectively ($\Delta\delta=\Delta\theta=10°$) and the *d* distance from *y*=+10 (Å) to −6 (Å) (Δd=2 Å), were calculated. Once this orientation was fixed *23*DMN was approached to *HP*CD along the y coordinate from 20 (Å) through −20 (Å) at Δd=0.5 Å. Each structure generated was solvated and optimized.

Binding energies as a function of the *d* distance (along the *y* coordinate) between *23*DMN and *HP*CD (polar and non-polar approaches) for three systems are depicted in Fig. 9. Calculations suggest that the complexation processes are favorable. Van der Waals interactions are mostly responsible for the complexation, while the electrostatics are insignificant at any host guest distance. The inclusion

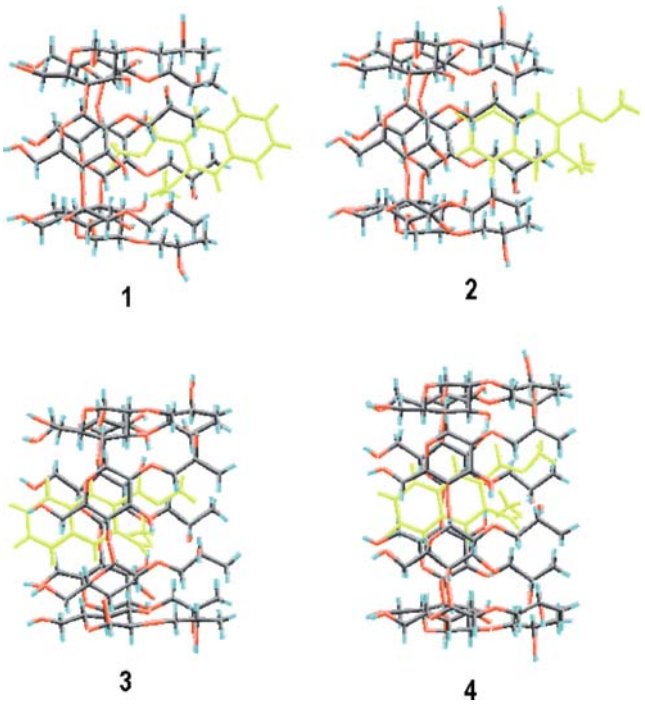

Fig. 10 MBE structures for the (1:1) *23*DMN complexes with α*HP*CD (*1* and *2*), β*HP*CD (*3*) and γ*HP*CD (*4*) obtained from representation depicted in Fig. 9

process of *23*DMN into the α*HP*CD, due to its small cavity size, however, is accompanied by a large energetic gap. This does not occur with the complexation of the other two *HP*CDs, where the guest seems to favorably pass through the cavity, especially on the NP side. As a consequence the minima binding energy conformation structures for *23*DMN:α*HP*CD are reached at relatively large *y* values (5.6 and 7.6 Å for both NP and P approaches respectively). For these structures a portion of *23*DMN is outside the cavity and exposed to the water. Nevertheless, this portion is considerably smaller than it is when *23*DMN complexes with its counterpart αCD [49]. However, *23*DMN is located inside the β- or γ*HP*CD and perfectly shielded from the solvent (y=−1.6 and 0.3 Å respectively). These structures, depicted in Fig. 10, are in agreement with most of the experimental fluorescence and dichroism circular findings.

Conclusions

*23*DMN forms complexes of stoichiometry 1/1 with α-, β- and γ*HP*CDs. The stability constants for the complexes with α- and γ*HP*CDs are somewhat larger than those for complexes formed with their naturally occurring counterparts α- and γCDs. Similar association constants for 23MN with β*HP*CD or βCD complexes were obtained. Whereas the signs of ΔH^0 match those obtained with their unsubstituted counterparts, their absolute values are smaller, as a consequence of the probably weaker guest/host interactions due to their larger cavity sizes. Favourable ΔS^0 for the three complexes could account for a good penetration of *23*DMN inside de *HP*CDs cavities. Nevertheless, in case of α*HP*CD, whereas tightly bonded to it, the inclusion may be not total. The latest statements will agree with the effective dielectric constant estimated when *23*DMN complexes with α*HP*CD, but also with R_∞ values and the quenching and circular dichroism experiments. Experimental results are also in agreement with a total penetration of *23*DMN inside β- and γ*HP*CD. MM calculations showed that 1:1 complexes of *23*DMN with *HP*CDs are capable of forming and that the non-bonded van der Waals interactions are mainly responsible for complex stability. Minima binding structures for the complexes nicely corroborates experimental finding.

Acknowledgements This research was supported by the Comunidad de Madrid (CAM project: S-055/MAT/0227), CICYT (project CTQ2005-04710/BQU) and Consejería de Educación y Ciencia de la Junta de Castilla-La Mancha (grant to M.J.G-A). We are grateful to Dr. Krois from the University of Vienna for the time he dedicated to us (M.J.G-A). We wish to express our thanks to M.L. Heijnen for assistance with the preparation of the manuscript.

References

1. Szejtli J, Osa T (1996) Comprehensive supramolecular chemistry, vol. 3. Cyclodextrins, Elsevier, Oxford
2. D'Souza VT, Lipkowitz KB (eds) (1998) Cyclodextrins. Chem Rev 98(5):1741–2076
3. Harada A (2001) Cyclodextrin-based molecular machines. Acc Chem Res 34:456–464
4. Nepogodiev SA, Stoddart JF (1998) Cyclodextrin-based catenanes and rotaxanes. Chem Rev 98(5):1959–1976
5. Flamigni L (1993) Inclusion of fluorescein and halogenated derivatives in α-, β-, and γ-cyclodextrins: a steady-state and picosecond time-resolved study. J Phys Chem 97(38):9566–9572
6. Fraiji EK Jr, Cregan TR, Werner TC (1994) Binding of 2-acetylnaphthalene to cyclodextrins studied by fluorescence quenching. Appl Spectrosc 48(1):79–84
7. Nakamura A, Sato S, Hamasaki K, Ueno A, Toda F (1995) Association of 1:1 inclusion complexes of cyclodextrins into homo- and heterodimers: a spectroscopic study using a TICT-forming fluorescent probe as a guest compound. J Phys Chem 99 (27):10959–10959
8. van Stam J, De Feyter S, De Schryver FC, Evans CH (1996) 2-naphthol complexation by b-cyclodextrin: influence of added short linear alcohols. J Phys Chem 100(51):19959–19966
9. Hamai S (1997) Inclusion of 2-chloronaphthalene by α-cyclodextrin and room-temperature phosphorescence of 2-chloronaphthalene in aqueous d-glucose solutions containing α-cyclodextrin. J Phys Chem B 101(9):1707–1712
10. Madrid JM, Villafruela M, Serrano R, Mendicuti F (1999) Experimental thermodynamics and molecular mechanics calculations of inclusion complexes of 9-methyl anthracenoate and 1-methyl pyrenoate with β-cyclodextrin. J Phys Chem B 103 (23):4847–4853
11. Sadlej-Sosnowska N, Siemiarczuk A (2001) A time resolved and steady-state fluorescence quenching study on naproxen and its cyclodextrin complexes in water. J Photochem Photobiol A: Chem 138:35–40
12. Di Marino A, Mendicuti F (2004) Thermodynamics of complexation of dimethyl esters of tere-, iso-, and phthalic acids with α- and β-cyclodextrins. Appl Spectrosc 58(7):823–830
13. Shannigrahi M, Bagchi S (2005) Time resolved fluorescence study of ketocyanine dye-b cyclodextrin interactions in aqueous and non-aqueous media. Chem Phys Lett 403(1–3):55–61
14. Turro NJ, Okubo T, Weed GC (1982) Enhancement of intramolecular excimer formation of 1,3-bichromophoric propanes via application of high pressure and via complexation with cyclodextrins. Protection from oxygen quenching. Photochem Photobiol 35(3):325–329
15. Kano K, Takenoshita I, Ogawa T (1982) g-Cyclodextrin-enhanced excimer fluorescence of pyrene and effect of *n*-butyl alcohol. Chem Lett Chem Soc Jpn 3:321–324
16. Hamai S (1989) Pyrene excimer formation in γ-cyclodextrin solutions: association of 1:1 pyrene-γ-cyclodextrin inclusion compounds. J Phys Chem 93(17):6527–6529
17. Pistolis G (1999) Dual excimer emission of *p*-terphenyl induced by g-cyclodextrin in aqueous solutions. Chem Phys Lett 304 (5,6):371–377
18. Sainz-Rozas PR, Isasi JR, González-Gaitano G (2005) Spectral and photophysical properties of 2-dibenzofuranol and its inclusion complexes with cyclodextrins. J Photochem Photobiol A: Chem 173(3):319–327
19. Catena GC, Bright FV (1989) Thermodynamic study on the effects of β-cyclodextrin inclusion with anilinonaphthalenesulfonates. Anal Chem 61(8):905–909

20. Madrid JM, Mendicuti F, Mattice WL (1998) Inclusion complexes of 2-methylnaphthoate and γ-cyclodextrin: experimental thermodynamics and molecular mechanics calculations. J Phys Chem B 102(11):2037–2044
21. Di Marino A, Mendicuti F (2002) Fluorescence of the complexes of 2-methylnaphthoate and 2-hydroxypropyl-α-, -β-, and -γ-cyclodextrins in aqueous solution. Appl Spectrosc 56(12):1579–1587
22. Pastor I, Di Marino A, Mendicuti F (2002) Thermodynamics and molecular mechanics studies on α- and β-cyclodextrins complexation and diethyl 2,6-naphthalenedicarboxylate guest in aqueous medium. J Phys Chem B 106(8):1995–2003
23. Muñoz de la Peña A, Ndou TT, Zung JB, Warner IM (1991) Stoichiometry and formation constants of pyrene inclusion complexes with β- and γ-cyclodextrin. J Phys Chem 95(8):3330–3334
24. Will AY, Muñoz de la Peña A, Ndou TT, Warner IM (1993) Spectroscopic studies of the interaction of *tert*-butylamine and *n*-propylamine with the β-cyclodextrin–pyrene complex. Appl Spectrosc 47(3):277–282
25. Madrid JM, Mendicuti F (1997) Thermodynamic parameters of the inclusion complexes of 2-methylnaphthoate and α- and β-cyclodextrins. Appl Spectrosc 51(11):1621–1627
26. Cervero M, Di Marino A, Mendicuti F (2000) Inclusion complexes of dimethyl 2,6-naphthalenedicarboxylate with α- and β-cyclodextrins in aqueous medium: thermodynamics and molecular mechanics studies. J Phys Chem B 104(7):1572–1580
27. Pastor I, Di Marino A, Mendicuti F (2005) Complexes of dihexyl 2,6-naphthalenedicarboxylate with α- and β-cyclodextrins: fluorescence and molecular modeling. J Photochem Photobiol A: Chem 173(3):238–247
28. Nelson G, Patonay G, Warner IM (1987) Fluorescence lifetime study of cyclodextrin complexes of substituted naphthalenes. Appl Spectrosc 41(7):1235–1238
29. Ferreira JAB, Costa SMB (2005) Non-radiative decay in rhodamines: role of 1:1 and 1:2 molecular complexation with β-cyclodextrin. J Photochem Photobiol A: Chem 173(3):309–318
30. Serna L, Di Marino A, Mendicuti F (2005) Inclusion complexes of a bichromophoric diester containing anthracene and naphthalene groups with alpha- and beta-cyclodextrins: thermodynamics and molecular mechanics. Spectrochim Acta Part A: Molec Biomolec Spectrosc 61(8):1945–1954
31. Hossain MA, Mihara H, Ueno A (2003) Fluorescence resonance energy transfer in a novel cyclodextrin–peptide conjugate for detecting steroid molecules. Bioorg Med Chem Lett 13(24):4305–4308
32. Park JW, Lee SY, Kim SM (2005) Efficient inclusion complexation and intra-complex excitation energy transfer between aromatic group-modified β-cyclodextrins and a hemicyanine dye. J Photochem Photobiol A: Chem 173(3):271–278
33. Nigam S, Durocher G (1997) Inclusion complexes of some 3H-indoles with cyclodextrins studied through excited state dynamics and steady state absorption and fluorescence spectroscopy. J Photochem Photobiol A: Chem 103(1,2):143–152
34. Krois D, Brinker UH (2006) Circular dichroism of cyclodextrin complexes. In: Dodziuk H (ed) Cyclodextrins and their complexes. Wiley-VCH, New York, pp 289–298 chapter 10.4
35. Murphy RS, Barros TC, Mayer B, Marconi G, Bohne C (2000) Photophysical and theoretical studies on the stereoselective complexation of naphthylethanols with β-cyclodextrin. Langmuir 16(23):8780–8788
36. Lipkowitz KB (1998) Applications of computational chemistry to the study of cyclodextrins. Chem Rev 98(5):1829–1873
37. Jursic BS, Zdravkovski Z, French AD (1996) Molecular modeling methodology of β-cyclodextrin inclusion complexes. J Mol Struct (Theochem) 366(1–2):113–117
38. Salvatierra D, Jaime C, Virgili A, Sanchez-Ferrando F (1996) Determination of the inclusion geometry for the β-cyclodextrin/benzoic acid complex by NMR and molecular modeling. J Org Chem 61(26):9578–9581
39. Madrid JM, Pozuelo J, Mendicuti F, Mattice WL (1997) Molecular mechanics study of the inclusion complexes of 2-methyl naphthoate with α- and β-cyclodextrins. J Colloid Interface Sci 193(1):112–120
40. Pozuelo J, Nakamura A, Mendicuti F (1999) Molecular mechanics study of the complexes of β-cyclodextrin with 4-(dimethylamino) benzonitrile and benzonitrile. J Incl Phenom Macroc Chem 35 (3):467–485
41. Cervello E, Mazzucchi F, Jaime C (2000) Molecular mechanics and molecular dynamics calculations of the β-cyclodextrin inclusion complexes with *m*-, and *p*-nitrophenyl alkanoates. J Mol Struct (Theochem) 530(1,2):155–163
42. Lino ACC, Takahata Y, Jaime C (2002) α- and β-cyclodextrin complexes with *n*-alkyl carboxylic acids and *n*-alkyl *p*-hydroxy benzoates. A molecular mechanics study of 1:1 and 1:2 associations. J Mol Struct (Theochem) 594(3):207–213
43. Pozuelo J, Mendicuti F, Mattice WL (1997) Inclusion complexes of chain molecules with cycloamyloses. 2. Molecular dynamics simulations of polyrotaxanes formed by Poly(ethylene glycol) and a-cyclodextrins. Macromolecules 30(12):3685–3690
44. Lipkowitz KB, Pearl G, Coner B, Peterson MA (1997) Explanation of where and how enantioselective binding takes place on permethylated β-cyclodextrin, a chiral stationary phase used in gas chromatography. J Am Chem Soc 119 (3):600–610
45. Köhler J, Hohla M, Söllner R, Eberle H-J (1998) Cyclohexadecanone derivative/γ-cyclodextrin complexes MD simulations and AMSOL calculations in vacuo and in aquo compared with experimental finding. Supramol Sci 5(1–2):101–116
46. Pozuelo J, Mendicuti F, Mattice WL (1998) Inclusion complexes of chain molecules with cycloamyloses. III. Molecular dynamics simulations of polyrotaxanes formed by polypropylene glycol and β-cyclodextrins. Polym J 30(6):479–484
47. Dodziuk H, Kozminski W, Lukin O, Sybilska D (2000) NMR manifestations and molecular dynamics modeling of chiral recognition of α-pinenes by α-cyclodextrin. J Mol Struct (Theochem) 525:205–212
48. Grabuleda X, Ivanov P, Jaime C (2003) Computational studies on pseudorotaxanes by molecular dynamics and free energy perturbation simulations. J Org Chem 68(4):1539–1547
49. Alvariza C, Usero R, Mendicuti F (2007) Binding of dimethyl 2,3-naphthalenedicarboxylate with α-, β- and γ-cyclodextrins in aqueous solution. Spectrochem Acta Part A 67(2):420–429
50. Di Marino A, Mendicuti F (2007) Rationalizing some experimental facts on the complexation of 2-methyl naphthalenecarboxylate and hydroxypropyled cyclodextrins by molecular mechanics and molecular dynamics. J Incl Phenom Macrocyc Chem 58 (3–4):295–305
51. Lakowicz JR (1999) Principles of fluorescence spectroscopy, 2nd edn. Kluwer, New York, p 298
52. Valeur B (2002) Molecular fluorescence: principles and applications. Wiley-VCH, Weinheim, p 89
53. Sybyl 6.9; Tripos Associates; St. Louis, Missouri, USA
54. Clark M, Cramer RC III, Van Opdenbosch N (1989) Validation of the general purpose Tripos 5.2 force field. J Comp Chem 10 (8):982–1012
55. MOPAC (AM1). Included in the Sybyl package
56. Brunel Y, Faucher H, Gagnaire D, Rasat A (1975) Program of minimization of the empirical energy of a molecule by a simple method. Tetrahedron 31(8):1075–1091
57. Press WH, Flannery BP, Teukolski SA, Vetterling WT (1988) Numerical recipes: the art of scientific computing. Cambridge University Press, Cambridge, p 312

58. Blanco M (1991) Molecular silverware. I. General solutions to excluded volume constrained problems. J Comp Chem 12(2):237–247
59. Platt JR (1949) Classification of spectra of cata-condensed hydrocarbons. J Chem Phys 17:484–495
60. Kodaka M (1998) Application of a general rule to induced circular dichroism of naphthalene derivatives complexed with cyclodextrins. J Phys Chem 102(42):8101–8103
61. Yorozu T, Hoshino M, Imamura M (1982) Fluorescence studies of pyrene inclusion complexes with α-, β-, and γ-cyclodextrins in aqueous solutions. Evidence for formation of pyrene dimer in γ-cyclodextrin cavity. J Phys Chem 86(22):4426–4429
62. Harata K, Uedaira H (1975) Circular dichroism spectra of the β-cyclodextrin complex with naphthalene derivatives. Bull Chem Soc Jpn 48(2):375–378
63. Shimizu H, Kaito A, Hatano M (1979) Induced circular dichroism of b-cyclodextrin complexes with substituted benzenes. Bull Chem Soc Jpn 52(9):2678–2684
64. Shimizu H, Kaito A, Hatano M (1981) Induced circular dichroism of β-cyclodextrin complexes with *o*-, *m*-, and *p*-disubstituted benzenes. Bull Chem Soc Jpn 54(2):513–519
65. Tinoco I Jr (1962) Theoretical aspects of optical activity. II. Polymers. Adv Chem Phys 4:113–60
66. Kodaka M (1991) Sign of circular dichroism induced by β-cyclodextrin. J Phys Chem 95(6):2110–2112
67. Kodaka M (1993) A general rule for circular dichroism induced by a chiral macrocycle. J Am Chem Soc 115 (9):3702–3705
68. Neckers DC, Volman DH, VonBünau G (1996) Advances in photochemistry. Wiley, New York, pp 5–35
69. Krois D, Brinker UH (1998) Induced circular dichroism and UV–vis absorption spectroscopy of cyclodextrin inclusion complexes: structural elucidation of supramolecular Azi-adamantane (Spiro[adamantane-2,3′-diazirine]). J Am Chem Soc 120(45): 11627–11632